Discrete gap solitons in binary positive-negative index nonlinear waveguide arrays with strong second-order couplings

Alexander A. Dovgiy[1,*] and Ilya S. Besedin[1,2]

[1]*Department of Solid State Physics and Nanosystems, National Research Nuclear University "MEPhI",*
Kashirskoe shosse 31, 115409 Moscow, Russia
[2]*Deutsches Elektronen-Synchrotron DESY, Notkestraße 85, 22607 Hamburg, Germany*

We report on the existence and properties of discrete gap solitons in zigzag arrays of alternating waveguides with positive and negative refractive indices. The zigzag quasi-one-dimensional configuration of the waveguide array introduces strong next-to-nearest neighbor interaction in addition to nearest neighbor coupling. Effective diffraction can be controlled both in size and in sign by the value of the next-to-nearest neighbor coupling coefficient and can even be canceled completely. In the regime where instabilities occur, we found different families of discrete solitons bifurcating from the gap edges of the linear spectrum. We show that both staggered and unstaggered discrete solitons can become highly localized states near the zero diffraction points even for low powers. Stability analysis has shown that the soliton solutions are stable over a wide range of parameters and can exist in focusing, defocusing, and even in an alternating focusing-defocusing array.

PACS number(s): 05.45.Yv, 42.82.Et, 78.67.Pt, 42.65.Tg

I. INTRODUCTION

Diffraction effects in discrete optical systems strongly differ from those in homogeneous and isotropic media. Peculiarities in diffraction effects appear due to rotational symmetry breaking into discrete optical systems, e.g., in arrays of waveguides, and canonical laws of diffraction cease to hold. Such systems allow one to control the diffraction either in size or in sign by the input conditions (angle of incidence of a beam) [1]. Diffractive beam spreading can even be arrested and diverging light can be focused. Analytical explanation of such phenomena comes from the mathematical relation between longitudinal and transverse wave number components of the wave vector. This relation is analogous to the dispersion relation in the temporal domain and describes the diffraction process in the system considered. In the case of waveguide arrays this relation is strictly periodic; hence, either strength or sign of diffraction depends on the transverse wave number component periodically, which in turn is determined by the tilt of the initial beam. Thus, the light beam can undergo both normal and anomalous diffraction and even can cross the array diffractionless. By using the diffraction properties of waveguide arrays, it is possible to produce structures with reduced, canceled, and even reversed diffraction. Results of experiments with such waveguide arrays are presented and compared with the predictions made by coupled-mode theory in [2]. Similar effects have been demonstrated in photonic crystals [3].

Diffraction effects play a significant role in the formation of spatial self-localized states (solitons) in nonlinear media. Discrete diffraction, as discussed above, has peculiarities and, as a result, nonlinear response in discrete structures demonstrates novel effects, which have no analogs in continuous systems. In nonlinear optical waveguide arrays (NOWAs) spatial discrete solitons can be formed due to the interplay between discrete diffraction, arising from linear coupling, and waveguide nonlinearity. Due to the possibility of diffraction management in waveguide arrays, different families of discrete solitons can be formed. Thus, both self-focusing and self-defocusing have been achieved experimentally in the same medium, structure (waveguide array), and wavelength [4]. Also, it was predicted analytically by Kivshar [5] that discrete self-focusing may be realized in an array of defocusing waveguides when the transverse wave number component of the wave vector lies at the edge of a Brillouin zone. Contrariwise, for the base of the Brillouin zone discrete self-focusing happened to be in an array of focusing waveguides [6]. All these listed features of discrete self-localized states (solitons) are consequences of the diffraction properties of the waveguide arrays mentioned above.

The studies discussed above are dedicated to the analysis of linear and nonlinear properties of uniform waveguide arrays, i.e., arrays composed of equally spaced identical waveguides. However, analysis of nonuniform waveguide arrays (binary arrays, arrays with defects, etc.) provides further degrees of freedom. Binary waveguide arrays possess a band gap, and may demonstrate symmetry breaking; thus, new kinds of discrete gap solitons can be obtained in such structures [7–15]. An interesting result was obtained in the case of a binary array with periodic switching of the coupling between successive waveguides (the coupling coefficients differ not only in modulus, but also in the sign); flat-top and kink solitons can be formed in this structure. Both stationary and "walking" gap solitons moving along the spatial coordinate with a tunable velocity exist for focusing, defocusing, and even alternating focusing-defocusing nonlinearities [16]. Efremidis and Christodoulides [17] proposed a zigzag configuration of the waveguide array that can exhibit strong second-order coupling in addition to the nearest neighbor coupling and this extended coupling affects the lattice dispersion relation within the Brillouin zone. As a result of this band alteration, completely different families of discrete solitons can be obtained, which are stable over a wide range of parameters. Also, diffraction management is studied in this structure and it can be employed to generate spatial discrete optical solitons at low power levels.

---

*Email address: dovgiyalexandr@gmail.com

The achievements of modern technologies, i.e., nanotechnologies, allow the manufacturing of artificial materials with unusual electromagnetic properties, i.e., metamaterials, which possess negative refraction in the microwave range [18–23], and more recently in the optical range without losses [24]. Compensation of energy losses in metamaterials can be achieved by implantation of components with active molecules or atoms into the structure of these artificial materials. The properties of negative index media can be employed in various new optical components for the integrated or fiber optics. The nonlinear response of such negative index metamaterials (NIMs) to the propagation of electromagnetic waves leads to novel optical phenomena and has been studied thoroughly in the last decade [25–27]. In particular, new regimes of nonlinear wave mixing between forward and backward waves can be brought about in NIMs [28–36] (for more examples of studies, see the review papers in [35,36]). Also, the interface between NIMs and positive index media (PIM) presents new features of refraction or localization of electromagnetic waves [37–41]. Interesting examples of mixed PIM-NIM structures providing forward-backward wave interaction are nonlinear oppositely directed couplers (NODCs) [42–45] and waveguide arrays with alternating PIM and NIM waveguides [46–50]. Unique features of nonlinear wave propagation, such as optical bistability [42], slit solitons [43,47,49], suppression of the modulation instability effect [44,48,50], and discrete gap solitons [45,46] were observed in these structures. In general, the model of PIM-NIM NOWA described by the coupled-mode equations can be applied to a broad range of metal-dielectric photonic structures, including plasmonic waveguides and metamaterials [51]. Energy localization can be significantly modified by introducing extended interactions (next-to-nearest neighbors) in PIM-NIM NOWAs. These extended interactions may be introduced by exploiting the topological arrangement of the lattice itself. The zigzag geometrical configuration provides the necessary deformation of the lattice leading to the emergence of second-order couplings in the PIM-NIM NOWA and completely different families of discrete soliton solutions can be obtained there in comparison with the ordinary first-order coupling PIM-NIM NOWA. Also, the dispersion relation of waves propagating in a zigzag PIM-NIM NOWA contains a band gap due to the alternating sign of the refractive index [49,50] that makes it different from the model considered in Ref. [17]. Thus, zigzag PIM-NIM NOWA provides further degrees of freedom for the manipulation of energy localization effects, diffraction management, and discrete solitons formation.

In a recent study, it was shown that the modulation instability effect in the zigzag PIM-NIM NOWA disappears regardless of the electromagnetic field power when the second-order coupling coefficient exceeds a certain threshold, the value of which depends on the transverse wave number component of the wave vector [50]. Thus, a uniform field distribution in the system in question can be both stable and unstable in the same nonlinear medium depending on the second-order coupling coefficient, and various regimes of nonlinear wave propagation are possible.

In this paper, we report on the existence of spatially localized modes for low powers in this quasi-one-dimensional waveguide array consisting of alternating positive index guides and negative index metamaterial guides. We show that the effective diffraction of the array can be controlled both in size and in sign, and can even be canceled at certain values of the second-order coupling coefficient. Zero diffraction points exist both at the base and at the edge of the Brillouin zone. Both staggered and unstaggered bright solitons can become highly localized states even at low power levels near these zero diffraction points. We perform stability analysis of these spatially localized states and demonstrate their stability over a wide range of parameters. We present the effects of nonlinear interaction of forward and backward waves in an example of a periodic photonic structure.

II. PHYSICAL MODEL

The coupling between second-order neighbors can be controlled by the angle θ between the perpendiculars connecting neighboring waveguides [17]. When the value of this angle is equal to π the second-order interactions are extremely weak and the system is reduced to a first-order interacting waveguide array. Reduction of this angle leads to the increase of the second-order coupling coefficient and the waveguide array takes a zigzag configuration (Fig. 1) (l is the distance between adjacent waveguides). Thus, zigzag NOWAs belong to a more general class of waveguide arrays which have extended interactions (beyond the nearest neighbors). The stationary field distribution in the physical system in question is described by the following nonlinear discrete differential equations [50]:

$$
\begin{aligned}
& i\partial_z a_n + \omega a_n + C_1(b_{n-1} + b_n) + C_2(a_{n-1} + a_{n+1}) \\
& \quad + \chi_1|a_n|^2 a_n = 0, \\
& -i\partial_z b_n + \omega b_n + C_1(a_n + a_{n+1}) \\
& \quad + C_2(b_{n-1} + b_{n+1}) + \chi_2|b_n|^2 b_n = 0,
\end{aligned}
\tag{1}
$$

where a_n and b_n are normalized field amplitudes in PIM and NIM waveguides, respectively, and $n = 0, \pm 1, \pm 2, \ldots$ is the number of the coupler in the array (see Fig. 1), and z is the propagation coordinate. C_1 and C_2 are first-order (nearest neighbor interaction) and second-order (next-to-nearest neighbor interaction) coupling coefficients, χ_1 and χ_2 are the normalized nonlinear susceptibilities of the PIM and NIM waveguides, respectively, and $\omega > 0$ is the phase mismatch between adjacent waveguides. Due to the opposite signs of the Poynting vectors in the PIM and NIM waveguides an effective feedback mechanism is introduced into the system under consideration and there is a minus sign in front of the spatial derivative in the second equation of the system (1) unlike the first equation. Therefore, the physical inputs for the
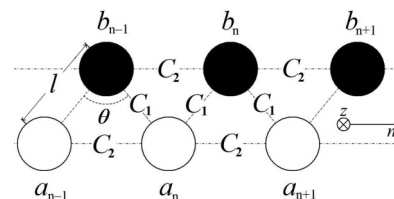

FIG. 1. Zigzag PIM-NIM NOWA (cross section). Empty circles indicate PIM waveguides; filled ones—NIM waveguides.

field amplitudes a_n and b_n are positioned at $z = 0$ and $z = L$, respectively, where L is the length of the array along the z direction. The boundary problem of the array in question can be simplified by considering stationary field distributions in waveguides [46] and, therefore, both fields can be given at $z = 0$ (i.e., b_n are given at their physical outputs).

We can determine the total power in the array as

$$P = \sum_n P_n = \sum_n (|a_n|^2 + |b_n|^2), \qquad (2)$$

as well as the Hamiltonian

$$H = 2\text{Re} \sum_n \{C_1(a_n b_n^* + a_n b_{n-1}^*) + C_2(a_n a_{n-1}^* + b_n b_{n-1}^*)$$

$$+ \frac{1}{4}(\chi_1|a_n|^4 + \chi_2|b_n|^4)\} + \omega P, \qquad (3)$$

from where one can obtain the equations of motion [Eq. (1)] via $i\dot{a}_n = -\partial H / \partial a_n^*$ and $i\dot{b}_n = \partial H / \partial b_n^*$ (an overdot stands for a derivative with respect to z). It is important to note that the Hamiltonian (3) and the total power (2) are conserved quantities of Eq. (1).

In order to derive the equations of motion in the so-called continuous approximation (i.e., slowly varying amplitudes), we consider the more general case of Eq. (1) describing a nonstationary field distribution in the linear array [49]:

$$i(\partial_z + \partial_t)a_n + \nu a_n + C_1(b_{n-1} + b_n) + C_2(a_{n-1} + a_{n+1}) = 0,$$

$$i(-\partial_z + \partial_t)b_n + \nu b_n + C_1(a_n + a_{n+1}) + C_2(b_{n-1} + b_{n+1}) = 0, \qquad (4)$$

where ν is a mismatch between propagation constants. One can easily obtain the linear part of Eq. (1) by substituting the stationary fields $a_n = a_n(z) \exp(-i\omega_{k,q}t)$ and $b_n = b_n(z) \exp(-i\omega_{k,q}t)$ into Eq. (4). Then, the phase mismatch ω will be defined as a sum of the mismatch between propagation constants ν and the frequency $\omega_{k,q}$. If we perform the Fourier transform with $a_n = \sum_{k,q} u_{k,q} \exp i(kz + qn - \omega_{k,q}t)$ and $b_n = \sum_{k,q} v_{k,q} \exp i(kz + qn + q/2 - \omega_{k,q}t)$, it is easy to obtain the following equation for the Fourier amplitudes: $\hat{L}_{k,q}\chi_{k,q} = 0$, where $\chi_{k,q} = (u_{k,q} \ v_{k,q})^T$,

$$\hat{L}_{k,q} = \begin{bmatrix} \omega - k + 2C_2 \cos q & 2C_1 \cos(q/2) \\ 2C_1 \cos(q/2) & \omega + k + 2C_2 \cos q \end{bmatrix}, \quad (5)$$

and $\omega = \omega_{k,q} + \nu$, from where one can easily obtain the dispersion relation of the system (4) via the equation $\det \hat{L}_{k,q} = 0$, which determines the frequency $\omega_{k,q}$ as a function of k and q:

$$\omega = -2C_2 \cos q \pm \sqrt{k^2 + 4C_1^2 \cos^2 q/2}. \qquad (6)$$

We can introduce the slowly varying amplitudes as follows:

$$a_n = \phi(z,t,n) \exp i(k_0 z + q_0 n - \omega_0 t),$$
$$b_n = \psi(z,t,n) \exp i(k_0 z + q_0 n - \omega_0 t), \qquad (7)$$

where ϕ and ψ are slowly varying functions; k_0, q_0, and $\omega_0 = \omega_{k_0,q_0}$ are spatial and temporal carrier frequencies, respectively. The frequencies of quasimonochromatic envelopes with narrow spectral widths slightly deviate from the carrier frequencies. From Eq. (7) it follows that the Fourier images of slowly

varying amplitudes satisfy the relations $\tilde{\chi}_{\tilde{k},\tilde{q}} = \chi_{k_0+\tilde{k},q_0+\tilde{q}}$ and $\hat{L}_{k_0+\tilde{k},q_0+\tilde{q}} \tilde{\chi}_{\tilde{k},\tilde{q}} = 0$, where $\tilde{\chi}_{\tilde{k},\tilde{q}} = (\phi_{\tilde{k},\tilde{q}} \ \psi_{\tilde{k},\tilde{q}})^T$, and $\tilde{k}, \tilde{q}$ are small deviations from the carrier frequencies. Hence, we have the following Taylor series expansion:

$$\left(\hat{L}_{k_0,q_0} + \tilde{k} \frac{\partial \hat{L}}{\partial \tilde{k}} \bigg|_{\tilde{k}=0} + \tilde{q} \frac{\partial \hat{L}}{\partial \tilde{q}} \bigg|_{\tilde{q}=0} + \frac{\tilde{q}^2}{2} \frac{\partial^2 \hat{L}}{\partial \tilde{q}^2} \bigg|_{\tilde{q}=0} + \cdots \right) \tilde{\chi}_{\tilde{k},\tilde{q}} = 0. \qquad (8)$$

Proceeding up to the fourth-order term in the Taylor series one can obtain equations for the slowly varying amplitudes ϕ and ψ (see Appendix) by applying the inverse Fourier transform to Eq. (8):

$$i\phi_z + i\phi_t + d_1^{(2)}\psi + iv_g^{(2)}\psi_x + d_2^{(2)}\psi_{2x} + id_3^{(2)}\psi_{3x} + d_4^{(2)}\psi_{4x}$$
$$+ d_1^{(1)}\phi + iv_g^{(1)}\phi_x + d_2^{(1)}\phi_{2x} + id_3^{(1)}\phi_{3x} + d_4^{(1)}\phi_{4x} = 0,$$

$$-i\psi_z + i\psi_t + d_1^{(2)}\phi + iv_g^{(2)}\phi_x + d_2^{(2)}\phi_{2x} + id_3^{(2)}\phi_{3x} + d_4^{(2)}\phi_{4x}$$
$$+ d_1^{(1)}\psi + iv_g^{(1)}\psi_x + d_2^{(1)}\psi_{2x} + id_3^{(1)}\psi_{3x} + d_4^{(1)}\psi_{4x} = 0, \qquad (9)$$

where x is a normalized coordinate ($n \to x$) [17], $\phi_{mx} = \frac{\partial^{(m)}\phi}{\partial x^{(m)}}$, $\psi_{mx} = \frac{\partial^{(m)}\psi}{\partial x^{(m)}}$ ($m = 1, \ldots, 4$), and the coefficients $d_1^{(1)} = 2C_2 \cos q_0$, $d_1^{(2)} = 2C_1 \cos(q_0/2)$,

$$v_g^{(1)} = 2C_2 \sin q_0, \quad v_g^{(2)} = C_1 \sin(q_0/2), \qquad (10)$$

$$d_2^{(1)} = C_2 \cos q_0, \quad d_2^{(2)} = \frac{C_1}{4} \cos(q_0/2), \qquad (11)$$

$$d_3^{(1)} = \frac{C_2}{3} \sin q_0, \quad d_3^{(2)} = \frac{C_1}{24} \sin(q_0/2), \qquad (12)$$

$$d_4^{(1)} = \frac{C_2}{12} \cos q_0, \quad d_4^{(2)} = \frac{C_1}{192} \cos(q_0/2). \qquad (13)$$

In the case of a stationary field distribution in the nonlinear array Eq. (9) can be written as

$$i\phi_z + \omega\phi + d_1^{(2)}\psi + iv_g^{(2)}\psi_x + d_2^{(2)}\psi_{2x} + id_3^{(2)}\psi_{3x}$$
$$+ d_4^{(2)}\psi_{4x} + d_1^{(1)}\phi + iv_g^{(1)}\phi_x + d_2^{(1)}\phi_{2x} + id_3^{(1)}\phi_{3x}$$
$$+ d_4^{(1)}\phi_{4x} + \chi_1|\phi|^2\phi = 0,$$
$$- i\psi_z + \omega\psi + d_1^{(2)}\phi + iv_g^{(2)}\phi_x + d_2^{(2)}\phi_{2x} + id_3^{(2)}\phi_{3x} + d_4^{(2)}\phi_{4x}$$
$$+ d_1^{(1)}\psi + iv_g^{(1)}\psi_x + d_2^{(1)}\psi_{2x} + id_3^{(1)}\psi_{3x} + d_4^{(1)}\psi_{4x}$$
$$+ \chi_2|\psi|^2\psi = 0. \qquad (14)$$

The latter equations [Eq. (14)] are the so-called continuous approximation of the discrete differential equations [Eq. (1)] when the field amplitudes are slowly varying functions with respect to the number of the coupler. The coefficients $v_g^{(1)}$ and $v_g^{(2)}$ can be attributed to the wave's spatial group velocity, and $d_j^{(i)}$ ($i = 1,2; j = 2,3,4$) represent the second-, third-, and fourth-order diffraction effects in the array, respectively.

III. DIFFRACTION RELATION AND MODULATION INSTABILITY

In Eq. (6) k and q are the longitudinal and transverse wave number components of the wave vector, respectively, and they are independent variables of the frequency function $\omega(k,q)$, that describes the dispersion in the array. To study the stationary field problem the frequency should be fixed; hence in this case Eq. (6) defines an implicit function $k(q)$, that can be expressed as

$$k^2(q) = (\omega + 2C_2 \cos q)^2 - 4C_1^2 \cos^2(q/2). \quad (15)$$

The latter expression (15) is the so-called diffraction relation and it can be used to carry out diffraction management in the array under consideration. Figure 2 depicts the diffraction curve in the domain of the first Brillouin zone. The second-order coupling coefficient significantly affects diffraction and, as a consequence, formation of bright solitons. As mentioned above, the second-order interactions in the array can be controlled by the angle between the perpendiculars connecting neighboring waveguides, and the system can be reduced to a first-order interacting array. In this case the second-order coupling coefficient is equal to zero and the diffraction relation takes the form considered in the ordinary PIM-NIM array [46]. It should be noted that we will only discuss the upper branch of the diffraction curve, since all results for the lower branch can be obtained from their upper branch counterparts by swapping negative index waveguides and positive index waveguides with each other. If q lies in the range $-\pi/2 < q < \pi/2$ the curvature of the diffraction relation is positive [$k''(q) > 0$] [Fig. 2(a)] and it has the form of a discrete Schrödinger-type (DS-type) diffraction [1,2,4,17], but reversed. In this region of q the effective diffraction of the array is "anomalous" and bright solitons are expected to arise in defocusing waveguides at the base of the Brillouin zone with eigenvalues lying in
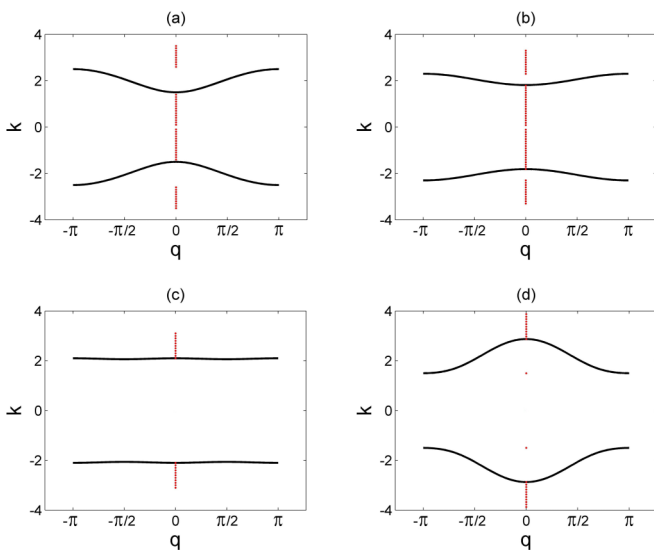

FIG. 2. (Color online) Diffraction curves (solid lines) for $C_2 = 0, 0.1, 0.2, 0.5$ shown in (a–d), respectively, with $C_1 = 1$, $\omega = 2.5$. Dots correspond to bright soliton solutions' eigenvalues lying in the band gaps.

the internal finite band gap. No bright solitons were observed in the focusing array in this case. However, when PIM and NIM waveguides have nonlinearities of different signs, it was observed that families of solitons bifurcate only from one of the edges of the band gap, e.g., for a focusing PIM and defocusing NIM only from the bottom, despite the fact that the finite gap edges are symmetric [46]. The nonlinearity breaks inversion symmetry in the reciprocal space. Contrariwise, in the regions $\pi/2 < |q| < \pi$ the curvature is negative [$k''(q) < 0$] and the effective diffraction of the array is "normal." Therefore, self-localization can become possible in focusing waveguides and bright soliton solutions may occur at the edge of the Brillouin zone with eigenvalues lying in the external semi-infinite band gap. In Ref. [46] it was found that there exists more than one family of symmetric and antisymmetric solitons bifurcating from the gap edges of the spectrum.

The increase of the second-order coupling coefficient leads to the finite band gap expansion and the curvature of the diffraction curve becomes lower for both the base and the edge of the Brillouin zone [Fig. 2(b)]. As a result, the bright soliton solutions become more localized (occupying a lower number of lattice sites) in comparison to those with smaller values of C_2 for the same power P. As can be seen in Fig. 2(d) the curvature of the diffraction curve changes its sign; i.e., it becomes negative ("normal" diffraction) in the region $-\pi/2 < q < \pi/2$ and positive ("anomalous" diffraction) in the regions $\pi/2 < |q| < \pi$ in comparison with Figs. 2(a) and 2(b). Thus, the effective diffraction of the array becomes like in the DS model when C_2 becomes commensurate with C_1. Bright solitons were observed only at the base of the Brillouin zone with eigenvalues lying in the external semi-infinite band gaps when the waveguides of the array in question were focusing. It is important to note that the so-called zero diffraction (zd) points [$k''(q) = 0$] exist there both at the base and at the edge of the Brillouin zone. To determine these zero diffraction points and appropriate values of C_2, we can use the Taylor series expansion of the diffraction relation (15) both at the base and at the edge of the Brillouin zone: $k^2 = (k_{q=0,\pi}^{(0)})^2 + 2\sum_{m=1}(-1)^m \delta_{q=0,\pi}^{(m)} q^{2m}/(2m)!$, where $\delta_{q=0}^{(m)} = 2^{2m} C_2^2 + 2\omega C_2 - C_1^2$ and $\delta_{q=\pi}^{(m)} = 2^{2m} C_2^2 - 2\omega C_2 + C_1^2$ are $(m+1)$th-order diffraction coefficients; $k_{q=0}^{(0)} = \pm[(\omega + 2C_2)^2 - 4C_1^2]^{1/2}$ and $k_{q=\pi}^{(0)} = \pm(\omega - 2C_2)$ are band edges at the base and at the edge of the Brillouin zone, respectively. Here, one can easily obtain the values of C_2 corresponding to the zero diffraction points of $(m+1)$th-order from the condition $\delta_{q=0,\pi}^{(m)} = 0$: $C_{2\,q=0}^{(m)zd} = [\sqrt{(\omega/2^m)^2 + C_1^2} - \omega/2^m]/2^m$ for the base and $C_{2\,q=\pi}^{(m)zd} = [\omega/2^m \pm \sqrt{(\omega/2^m)^2 - C_1^2}]/2^m$ for the edge of the Brillouin zone. For the values of parameters used in Fig. 2 ($C_1 = 1$, $\omega = 2.5$) we can estimate the values of C_2 under which the second-order effective diffraction in the array disappears: $C_{2\,q=0}^{(1)zd} \approx 0.175$ and $C_{2\,q=\pi}^{(1)zd} = 0.25, 1$. Hence, discrete solitons near zero diffraction points can be observed both at the base and at the edge of the Brillouin zone in contrast to the ordinary zigzag array studied in [17] where such nonlinear states were observed only at the edge of the Brillouin zone. This class of solutions with eigenvalues positioned deep inside the band

gap represents highly localized states occupying, in essence, one to three lattice sites. As the value of C_2 increases above 0.25 the diffraction curve becomes steeper and, as a result, the bright soliton solutions become less localized. Thus, the array under consideration provides further degrees of freedom for diffraction management and more ways to generate spatial discrete optical solitons at low power levels in comparison with the arrays considered in [17,46].

We investigate the modulation instability (MI) of the plane wave solution of Eq. (1), $a_n = a \exp i(kz + qn)$ and $b_n = b \exp i(kz + qn + q/2)$, with respect to small perturbations. The plane wave solution's amplitudes are coupled by the following equation, $2C_1 \cos(q/2)b = [k(q) - \omega - 2C_2 \cos q]a$, where $k(q)$ is determined by Eq. (15). The instability of perturbed continuous waves is closely related to the presence of spatial bright solitons and occurs in the system due to the interplay between nonlinear interaction and diffraction effects. Therefore, the presence of MI can be considered as a precursor to bright soliton formation. We investigate the linear stability by perturbing the amplitude and the phase of the solution as $a_n = (a + A_n) \exp i(kz + qn + \Phi_n)$ and $b_n = (b + B_n) \exp i(kz + qn + q/2 + \Psi_n)$, where $A_n(z)$, $B_n(z)$ and the differences $\Phi_n(z) - \Psi_n(z)$ are assumed to be small in comparison with the parameters of the plane wave solution. After the linearization of Eq. (1) in these small perturbations and applying the transformations $(A_n, \Phi_n) \equiv (A, \Phi) \exp i(Kz + Qn)$ and $(B_n, \Psi_n) \equiv (B, \Psi) \exp i(Kz + Qn + Q/2)$ for these quantities we obtain the following relation between the longitudinal K and the transverse Q wave number components of the perturbations' wave vector: $\hat{S}_Q \vec{g} = K \hat{E} \vec{g}$, where $\vec{g} = (A, \Phi, B, \Psi)^T$, $\hat{E}$ is a 4×4 unit matrix, and $\hat{S}_Q = \{s_{ij}\}$ ($i, j = 1, \dots, 4$) is referred to as the stability matrix which is used to investigate MI in the system in question. The coefficients of this 4×4 stability matrix are given by

$$s_{11} = -s_{22} = s_{33} = s_{44} = 2C_2 \sin q \sin Q,$$

$$s_{12} = -2i[C_1 b \cos(q/2) + 2C_2 a \cos q \sin^2(Q/2)],$$

$$-s_{13} = s_{31} = (-a/b)s_{24} = (b/a)s_{42} = 2C_1 \sin(q/2) \sin(Q/2),$$

$$(1/b)s_{14} = bs_{41} = (-a)s_{23} = (-1/a)s_{32}$$
$$= 2iC_1 \cos(q/2) \cos(Q/2),$$

$$s_{21} = -i[3\chi_1 a^2 + \omega - k(q) + 2C_2 \cos q \cos Q]/a,$$

$$s_{34} = 2i[C_1 a \cos(q/2) + 2C_2 b \cos q \sin^2(Q/2)],$$

$$s_{43} = i[3\chi_2 b^2 + \omega + k(q) + 2C_2 \cos q \cos Q]/b.$$

MI occurs when at least one of the stability matrix's eigenvalues possesses a nonzero imaginary part which results in an exponential growth of the phase and the amplitude of the plane wave solution with the perturbations. To find the eigenvalues of $\hat{S}_Q$ one should solve the equation $\det \| \hat{S}_Q - K\hat{E} \| = 0$. We performed numerical diagonalization of the stability matrix and determined the regions where the plane wave solution is stable or unstable as a function of q and C_2 in the focusing array under consideration. Herein, MI is totally absent at the base

of the Brillouin zone ($q = 0$) when $0 \leqslant C_2 \leqslant C_{2q=0}^{(1)zd} \approx 0.175$. At $C_2 > C_{2q=0}^{(1)zd}$, the plane wave solution appears to be unstable [Fig. 3(a)]. At the vicinity of the edge of the Brillouin zone ($q \cong \pi$) MI occurs when $0 \leqslant C_2 < C_{2q=\pi}^{(1)zd} = 0.25$ and is totally absent when $C_{2q=\pi}^{(1)zd} \leqslant C_2$ [Fig. 3(b)]. These results are in full agreement with the conclusions previously drawn from the linear diffraction diagram.

IV. DISCRETE SOLITONS

In this section we will investigate the existence and stability of bright soliton solutions that are the self-localized states along the transverse discrete direction of the array in question. In the continuous approximation these solitons can be described by a nonlinear Schrödinger-type equation [Eq. (14) when $d_3^{(1,2)}$ and $d_4^{(1,2)}$ are negligible], but only for broad enough beams with narrow spectral widths. If we want to examine the existence and properties of highly localized states with good precision, it will be necessary to perform numerical analysis of the discrete Eq. (1). As discussed above, the discrete solitons can bifurcate in the band gaps from the gap edges if the necessary balance between the diffraction and nonlinear interaction takes place. In order to carry out an analytical investigation we will perform the standard multiple-scale expansion procedure as in [46]. We are interested in discrete soliton solutions of Eq. (1) having the form $a_n(z) = u_n \exp i(\kappa z + qn)$, $b_n(z) = v_n \exp i(\kappa z + qn)$, where u_n and v_n are real and vanish as $n \to \pm\infty$, κ is the solution's eigenvalue, and two cases of particular interest—unstaggered and staggered solutions, i.e., $q = 0$ and π, respectively, will be treated separately in the rest of this section.

A. At the base of the Brillouin zone: $q = 0$

In this case Eq. (1) is reduced to the following system of nonlinear algebraic equations:

$$(\omega - \kappa)u_n + C_1(v_{n-1} + v_n) + C_2(u_{n-1} + u_{n+1})$$
$$+ \chi_1|u_n|^2 u_n = 0,$$
$$(\omega + \kappa)v_n + C_1(u_n + u_{n+1}) + C_2(v_{n-1} + v_{n+1})$$
$$+ \chi_2|v_n|^2 v_n = 0. \qquad (16)$$

We are interested in the solutions with exponential decay at $n \to -\infty$ ($n \to +\infty$); hence, we can require the relation $u_{n+1}/u_n = v_n/v_{n-1} = \alpha$ ($u_n/u_{n+1} = v_{n-1}/v_n = \alpha$) to hold, where α is real and $|\alpha| > 1$. For exponentially decaying solutions the nonlinear terms of Eq. (16) can be neglected at large n, and by substituting the latter expression to Eq. (16) one can easily obtain the relation which establishes the domains of the solution's eigenvalue κ, where solitons exist: $[(\omega - \kappa)\alpha + C_2(1 + \alpha^2)][(\omega + \kappa)\alpha + C_2(1 + \alpha^2)] = C_1^2 \alpha (1 + \alpha)^2$. The results of the numerical analysis of this fourth-order algebraic equation are depicted in Fig. 2 with dots. In order to satisfy the condition $|\alpha| > 1$, the soliton solution's eigenvalues should be located in the band gaps where the light propagation is forbidden [Figs. 2(a) and 2(b)]. At some values of the second-order coupling coefficient C_2 the internal finite band gap domain of the soliton solutions' eigenvalues may be degenerate [Figs. 2(c) and 2(d)].
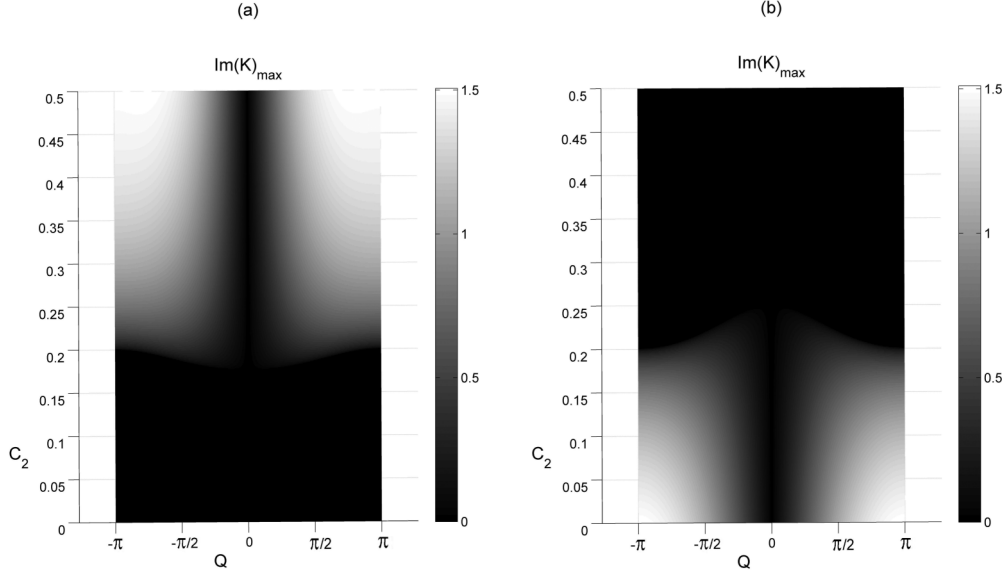
FIG. 3. Modulation instability growth rate (maximum imaginary part of the stability matrix's eigenvalues) vs Q and C_2, with $a = 1$, $\chi_1 = \chi_2 = 1$, $C_1 = 1$, $\omega = 2.5$. Panel (a) corresponds to $q = 0$; (b) corresponds to $q \cong \pi$.

To consider the bifurcation of solitons from the gap edges, we will shift the soliton solution's eigenvalue towards the gap: $\kappa = k_{q=0}^{(0)} + \kappa_2 \varepsilon^2$, where $k_{q=0}^{(0)}$ indicates gap edges as were determined in the previous section, $\varepsilon \ll 1$ is a small parameter characterizing the shift of the eigenvalue towards the gap, and the sign of κ_2 determines the direction of the shift. Performing standard multiple-scale series expansion $u_n = \varepsilon \sum_{m=0} \varepsilon^m U_m(x)$ and $\upsilon_n = \varepsilon \sum_{m=0} \varepsilon^m V_m(x)$, where $x = \varepsilon n$, we obtain the relation $V_0 = \beta U_0$, where $\beta = [k_{q=0}^{(0)} - (\omega + 2C_2)]/2C_1 < 0$. Proceeding up to the third-order term in the multiple-scale series we obtain the following stationary nonlinear Schrödinger (NLS) equation:

$$\gamma \frac{d^2 U_0}{dx^2} - \kappa_2 (1 - \beta^2) U_0 + (\chi_1 + \beta^4 \chi_2) U_0^3 = 0, \qquad (17)$$

where $\gamma = \beta C_1/2 + C_2(1 + \beta^2)$ can be interpreted as the second-order diffraction coefficient. Note that γ is equal to zero when $C_2 = C_{2q=0}^{(1)zd}$. Equation (17) has a well-known bright soliton solution,

$$U_0 = A / \cosh(bx), \qquad (18)$$

where $A = [2\kappa_2(1 - \beta^2)/(\chi_1 + \beta^4 \chi_2)]^{1/2}$ and $b = [\kappa_2(1 - \beta^2)/\gamma]^{1/2}$. When $C_2 < C_{2q=0}^{(1)zd}$ the second-order diffraction coefficient γ is negative and $(1 - \beta^2)$ is positive (negative) for the upper (lower) branch of the spectrum. Thus, from the expression for b, the shift of the soliton's eigenvalue should be towards the internal finite band gap [i.e., $\kappa_2 < 0$ ($\kappa_2 > 0$) for the upper (lower) branch of the spectrum], and at the same time, from the expression for A the quantity $(\chi_1 + \beta^4 \chi_2)$ must be negative. But for the PIM and NIM waveguides with focusing nonlinearities, this condition cannot be satisfied; hence, no bright solitons can bifurcate from the gap edges when all the waveguides are focusing. In fact, this conclusion can be drawn directly from Eq. (17) and is in good agreement with the results depicted in Figs. 2(a) and 2(b) and the fact that the effective diffraction of the array

is anomalous in this case. The numerical solution associated with this case is depicted in Fig. 6(a). Meanwhile, bright solitons are expected to exist in the finite gap when the PIM and NIM waveguides have nonlinearities of different signs; e.g., when $\chi_1 = -1$ and $\chi_2 = 1$ the quantity $(\chi_1 + \beta^4 \chi_2)$ is negative for the top of the finite gap and positive (no solitons) for the bottom of the finite gap and the other way round when $\chi_1 = 1$ and $\chi_2 = -1$, despite the fact that the gap edges are symmetric (this feature is reminiscent of the inversion symmetry breaking in the reciprocal space, reported in [46]). If $C_2 > C_{2q=0}^{(1)zd}$ the second-order diffraction coefficient γ is positive. Thus, from the expression for b, the shift of the soliton's eigenvalue should be towards the external semi-infinite band gaps [i.e., $\kappa_2 > 0$ ($\kappa_2 < 0$) for the upper (lower) branch of the spectrum], and at the same time, from the expression for A the quantity $(\chi_1 + \beta^4 \chi_2)$ must be positive. Hence, bright solitons exist in the focusing array in this case and it is consistent with the fact that the effective diffraction of the array is normal [Figs. 2(c) and 2(d)].

The numerical results have shown that more than one soliton family bifurcates from the gap edges of the linear spectrum [Figs. 5(a) and 5(c)]. The deeper the soliton's eigenvalue lies in the band gap, the more localized the solitons are [Fig. 5(e)] and the higher the corresponding power level is [Fig. 4]. But near the zero diffraction points these soliton solutions can be highly localized states even with the eigenvalues closely located to the gap edges, hence, at low power levels [Fig. 5(a)].

In Fig. 4 the power P associated with bright soliton numerical solutions is depicted as a function of the eigenvalue κ for the base and for the edge of the Brillouin zone. In both cases the behavior of the $P(\kappa)$ is like the one in the standard discrete NLS model [17]. For relatively small values of power and weakly localized solutions, the behavior of $P(\kappa)$ can be approximately described within the NLS limit. Using Eq. (2) and the expression (18) for the bright soliton solution with $q = 0$ in the continuous approximation, the $P(\kappa)$ curve can be approximately described
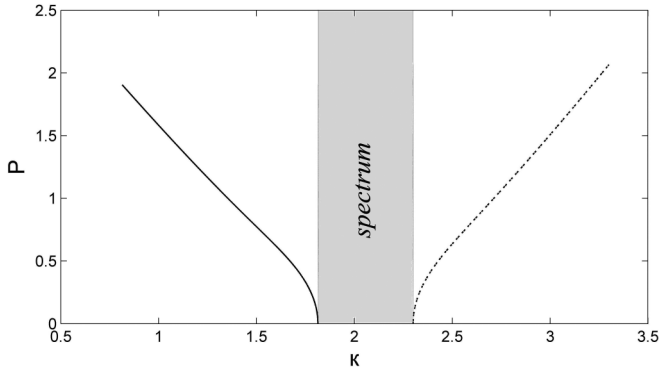
FIG. 4. Power P vs κ curve of stable bright solitons in defocusing array at $q = 0$ (solid line) and in focusing array at $q = \pi$ (dashed line) with $\omega = 2.5$, $C_1 = 1$, $C_2 = 0.1$.

by $P \approx 4(1 + \beta^2)[\gamma(1 - \beta^2)(\kappa - k_{q=0}^{(0)})]^{1/2}/|\chi_1 + \beta^4\chi_2|$ at the base of the Brillouin zone. On the other hand, for high power levels and strongly localized solutions, most of the power is confined in one waveguide, and, therefore, $P \approx 2(1 - \beta^4)(\kappa - k_{q=0}^{(0)})/(\chi_1 + \beta^4\chi_2)$ for the solutions with $q = 0$. These two approximated dependences can be easily seen in Fig. 4. No peculiarities occur with the change of C_2 in the behavior of $P(\kappa)$ and these two approximations remain valid. Thus, the deeper the soliton's eigenvalue lies in the band gap, the larger the relative difference $(\kappa - k_{q=0}^{(0)})$ is and the higher the power P is.

Now we will examine the stability of these bright soliton solutions with the linear stability analysis. We introduce perturbations in the exact solution, $a_n = u_n \exp(i\kappa z)$ and $b_n = \upsilon_n \exp(i\kappa z)$, in a fashion $a_n = [u_n + (U_n + Q_n)\exp(i\Lambda z) + (U_n - Q_n)\exp(-i\Lambda z)]\exp(i\kappa z)$ and $b_n = [\upsilon_n + (V_n + W_n)\exp(i\Lambda z) + (V_n - W_n)\exp(-i\Lambda z)]\exp(i\kappa z)$, where U_n, Q_n, V_n, and W_n are assumed to be small in comparison with u_n and υ_n. Substituting these perturbed solutions to Eq. (1) and linearizing Eq. (1) in small perturbations we arrive at the following coupled eigenvalue problem:

$$-kQ_n + \omega Q_n + K_1(W_{n-1} + W_n) + K_2(Q_{n-1} + Q_{n+1}) + \chi_1 u_n^2 Q_n = \Lambda U_n,$$

$$-kU_n + \omega U_n + K_1(V_{n-1} + V_n) + K_2(U_{n-1} + U_{n+1}) + 3\chi_1 u_n^2 U_n = \Lambda Q_n,$$

$$-kW_n - \omega W_n - K_1(Q_{n+1} + Q_n) - K_2(W_{n-1} + W_{n+1}) - \chi_2 \upsilon_n^2 W_n = \Lambda V_n,$$

$$-kV_n - \omega V_n - K_1(U_{n+1} + U_n) - K_2(V_{n-1} + V_{n+1}) - 3\chi_2 \upsilon_n^2 V_n = \Lambda W_n.$$

When all eigenvalues Λ are real the solution is stable, whereas, if an eigenvalue possesses a nonzero imaginary part the solution becomes unstable. We have analyzed this problem numerically. As can be seen from Figs. 5(a) and 5(c), solitons with different values of power P exist in the array at the same parameters of the system. The explanation comes from Eq. (17). Indeed, the amplitudes U_0 and V_0 can be centered either at a PIM [Fig. 5(a)] or at a NIM [Fig. 5(c)] waveguide, thus giving two different families of soliton solutions which differ in the power level. The stability analysis has shown that the soliton solution with higher power level (excited state) is unstable [Fig. 5(d)]. The eigenvalue problem has complex roots Λ with nonzero imaginary parts leading to an exponential growth of the amplitudes of the small perturbations on the soliton's background. The bright soliton solutions with lower power levels (ground state) are stable over the wide range of parameters of the system in question [Figs. 5(b), 5(f), and 6(b)]. All the eigenvalues Λ are real, the instability does not occur, and the perturbations are the small oscillations on the top of the soliton's background.

B. At the edge of the Brillouin zone: $q = \pi$

Here we will study the properties of staggered soliton solutions, i.e., $q = \pi$. One can easily obtain the equations for these solutions from Eq. (16) by making the change of variables $u_n \to (-1)^n u_n$, $\upsilon_n \to (-1)^n \upsilon_n$, and consequently, $\alpha \to -\alpha$. It is obvious that the relation which establishes domains of the solution's eigenvalue for which solitons exist does not change. Hence, suitable eigenvalues of staggered solitons lie in the band gaps, too. To perform the multiple-scale analysis for

this case we should also shift the soliton solution's eigenvalue towards the gaps. The only difference is that the gap edges should be taken at $q = \pi$. Thus, we consider $\kappa = k_{q=\pi}^{(0)} + \kappa_2\varepsilon^2$, where $k_{q=\pi}^{(0)}$ indicate gap edges as were determined in Sec. III at the edge of the Brillouin zone. The first-order term of the multiple-scale series gives that at the positive (negative) gap edge $V_0 = 0$, $U_0 \neq 0$, and $V_1 = [C_1/2(\omega - 2C_2)]dU_0/dx$ ($U_0 = 0$, $V_0 \neq 0$, and $U_1 = -[C_1/2(\omega - 2C_2)]dV_0/dx$), i.e., field amplitudes in PIM and NIM waveguides have different orders of magnitude [see Figs. 6(c), 7(a), and 7(c)]. Proceeding up to ε^3 we arrive at the stationary NLS equation for the positive (negative) gap edge:

$$\sigma \frac{d^2 U_0}{dx^2} - \kappa_2 U_0 + \chi_1 U_0^3 = 0 \quad \left(\sigma \frac{d^2 V_0}{dx^2} + \kappa_2 V_0 + \chi_2 V_0^3 = 0\right),$$

(19)

where $\sigma = (4C_2^2 - 2\omega C_2 + C_1^2)/2(\omega - 2C_2)$ can be interpreted as the second-order diffraction coefficient by analogy with γ and it is equal to zero when $C_2 = C_{2q=\pi}^{(1)zd}$. Note that in Eq. (19) only the nonlinearity of PIM (NIM) waveguides has influence due to the different field magnitudes' orders. The bright soliton solution of Eq. (19) is $U_0 = B/\cosh(ax)$ [$V_0 = B/\cosh(ax)$], where $B = [2\kappa_2/\chi_1]^{1/2}$ and $a = [\kappa_2/\sigma]^{1/2}$ ($B = [-2\kappa_2/\chi_2]^{1/2}$ and $a = [-\kappa_2/\sigma]^{1/2}$) for the positive (negative) gap edge. When $C_2 < C_{2q=\pi}^{(1)zd}$ the bright solitons bifurcate from the gap edges towards the external semi-infinite gaps in the focusing array [Figs. 7(a) and 7(c)] because σ is positive and the effective diffraction of the array is normal at the edge of the Brillouin zone [Figs. 2(a) and 2(b)]. On the contrary, no bright
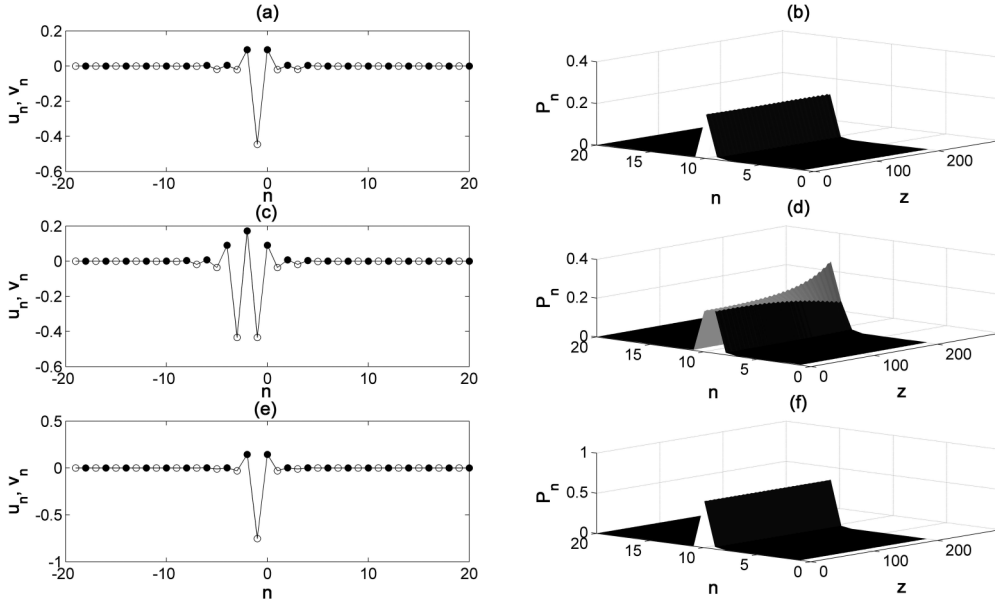
FIG. 5. Unstaggered discrete solitons with different eigenvalues within the positive infinite gap: (a) $\kappa = 2.3$, (c) $\kappa = 2.3$ (unstable excited state) and (e) $\kappa = 2.7$; and the corresponding power evolution depicted in (b), (d), (f), respectively, in the focusing array ($\chi_{1,2} = 1$) with $\omega = 2.5$, $C_1 = 1$, $C_2 = 0.2$. The infinite gaps are $|\kappa| > 2.1$. Empty (filled) circles indicate PIM (NIM) waveguides.

solitons can bifurcate from the gap edges in the focusing array when $C_2 > C_{2_{q=\pi}}^{(1)zd}$.

In this case the effective diffraction of the array is anomalous [Fig. 2(d)], σ is negative, and the staggered bright solitons exist in the defocusing array [Fig. 6(c)] with eigenvalues lying near the finite gap edges [Fig. 2(d)]. Using the analytical expressions for the solutions of Eq. (19) bifurcating from the positive (negative) gap edge at $q = \pi$ and Eq. (2), we can approximately describe the $P(\kappa)$ curve by $P = 4[(\kappa - k_{q=\pi}^{(0)})\sigma]^{1/2}/|\chi_1| + C_1^{2}(\kappa - k_{q=\pi}^{(0)})^{3/2}/3(\omega - 2C_2)^2|\chi_1|\sigma^{1/2}$ ($P = 4[(k_{q=\pi}^{(0)} - \kappa)\sigma]^{1/2}/|\chi_2| + C_1^{2}(k_{q=\pi}^{(0)} - $

$\kappa)^{3/2}/3(\omega - 2C_2)^2|\chi_2|\sigma^{1/2}$) at low power levels. For strongly localized solutions at large values of power the $P(\kappa)$ curve can be approximately described by $P = 2(\kappa - k_{q=\pi}^{(0)})/\chi_1$ [$P = 2(k_{q=\pi}^{(0)} - \kappa)/\chi_2$] [Fig. 4]. As the eigenvalue goes deeper into the band gap the power increases and the staggered solitons become more localized.

The stability of these staggered soliton solutions is investigated similarly to the stability of unstaggered soliton solutions as was performed in the previous subsection. As can be seen from Figs. 7(a) and 7(c), symmetric and antisymmetric staggered soliton families exist in the array at the same parameters
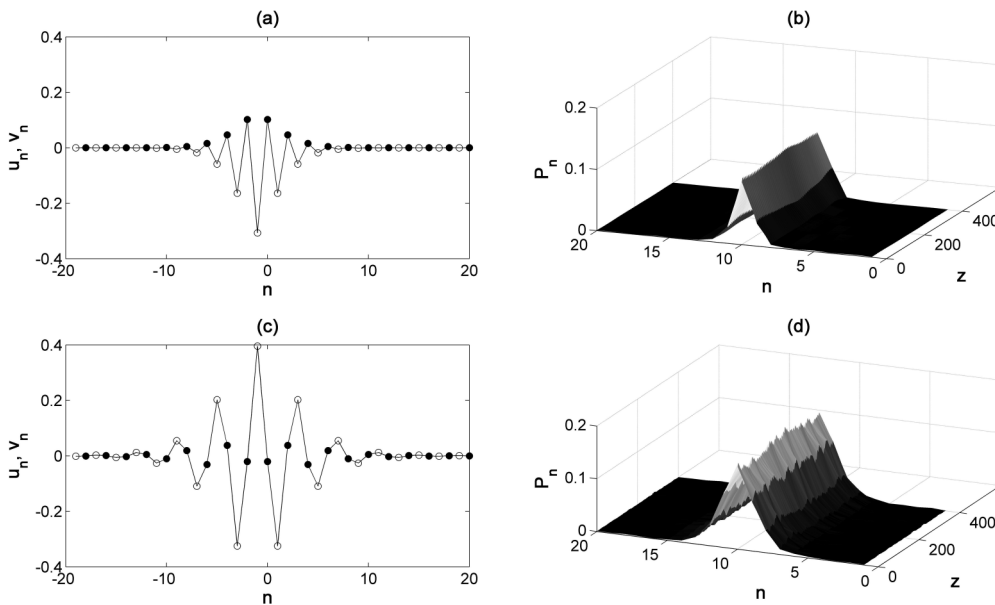

FIG. 6. Unstaggered (a) and staggered (c) discrete solitons in the finite gap with $\kappa = 1.9$ when $C_2 = 0.15$ and with $\kappa = 1.43$ when $C_2 = 0.5$, respectively, and the corresponding power evolution depicted in (b), (d), respectively, in the defocusing array ($\chi_{1,2} = -1$) with $\omega = 2.5$, $C_1 = 1$.
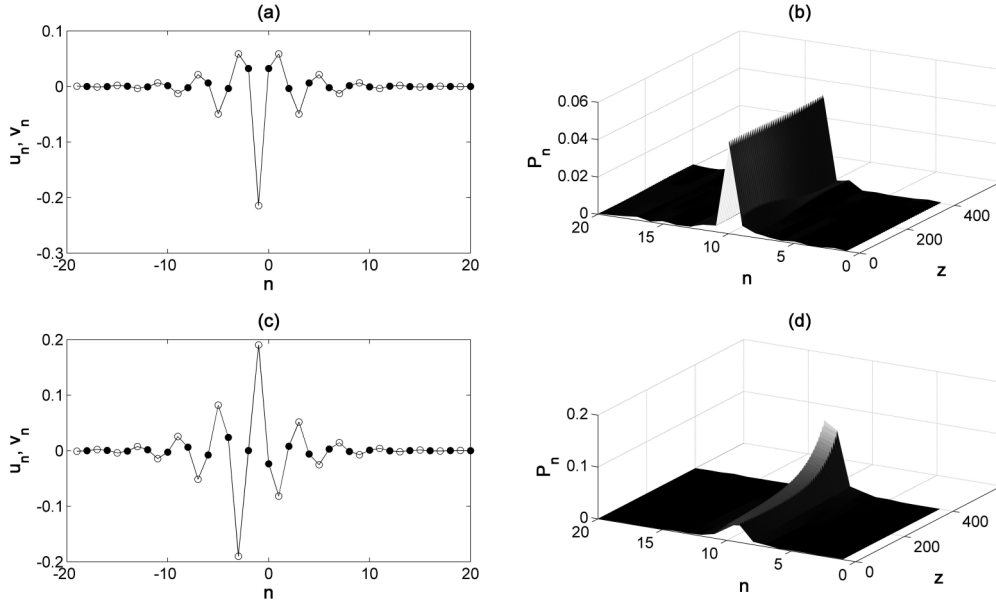
FIG. 7. Staggered discrete solitons in the positive infinite gap: (a) stable symmetric state and (c) unstable antisymmetric state; the corresponding power evolution is depicted in (b,d), respectively, in the focusing array ($\chi_{1,2} = 1$) with $\omega = 2.5$, $C_1 = 1$, $C_2 = 0.19$, $\kappa = 2.14$. The infinite gaps are $|\kappa| > 2.12$.

of the system. Numerical stability analysis has shown that the antisymmetric state is unstable [Fig. 7(d)]. The symmetric staggered solitons are stable both in focusing and in defocusing arrays [Figs. 7(b) and 6(d)]. The physical reason for this behavior is that the antisymmetric soliton is an excited state with higher power levels in comparison with symmetric soliton.

V. CONCLUSIONS

In this paper, we report on the existence and properties of discrete gap solitons in a binary nonlinear waveguide array of alternating positive and negative index waveguides with extended interactions. The zigzag geometrical configuration of the array in question allows introducing extended strong second-order (next-to-nearest neighbor) couplings in addition to the first-order (nearest neighbor) coupling. The controllability of this second-order coupling allows managing the diffraction properties of this array. The effective diffraction can be controlled both in size and in sign; it can be both normal and anomalous in the same system and even zero diffraction points exist at certain values of the second-order coupling coefficient. We have investigated modulation instability in the focusing array and determined the regions where the continuous wave solution is stable or unstable as a function of the spatial Bloch momentum vector and the second-order coupling coefficient. Modulation instability does not occur in regions of anomalous diffraction, whereas in regions of normal diffraction the continuous waves are unstable both at the base and at the edge of the Brillouin zone. Due to the alternating positive and negative index waveguides the linear

spectrum has band gaps giving origin to more than one bright soliton family bifurcating from the gap edges. The discrete solitons with the lowest power level are stable over a wide range of parameters. Discrete self-focusing is observed both in the focusing and in the defocusing array, and even in the alternating focusing-defocusing array; moreover, near the zero diffraction points the highly localized states are possible at low power levels both at the base and at the edge of the Brillouin zone. Thus, the array considered is a more general model combining the properties of the arrays considered in Refs. [17,46], and provides more ways to manipulate energy localization effects, spatial discrete solitons formation, and exert diffraction management.

APPENDIX

In this Appendix we detail, in order to justify the order of development and for sake of completeness, our calculations between Eqs. (8) and (9). Proceeding up to the fourth-order term in Eq. (8) and combining all terms of the equation into a single 2×2 matrix we have the following equation:

$$\hat{L} \tilde{\chi}_{\tilde{k},\tilde{q}} = 0, \qquad (A1)$$

where

$$L_{11} = \omega_{\tilde{k},\tilde{q}} + \nu - \tilde{k} + 2C_2 \cos q_0 - 2C_2 \sin q_0 \tilde{q} - 2C_2 \cos q_0 \frac{\tilde{q}^2}{2} + 2C_2 \sin q_0 \frac{\tilde{q}^3}{6} + 2C_2 \cos q_0 \frac{\tilde{q}^4}{24},$$

$$L_{12} = L_{21} = 2C_1 \cos\left(\frac{q_0}{2}\right) - C_1 \sin\left(\frac{q_0}{2}\right)\tilde{q} - \frac{C_1}{2}\cos\left(\frac{q_0}{2}\right)\frac{\tilde{q}^2}{2} + \frac{C_1}{4}\sin\left(\frac{q_0}{2}\right)\frac{\tilde{q}^3}{6} + \frac{C_1}{8}\sin\left(\frac{q_0}{2}\right)\frac{\tilde{q}^4}{24},$$

$$L_{22} = \omega_{\tilde{k},\tilde{q}} + \nu + \tilde{k} + 2C_2 \cos q_0 - 2C_2 \sin q_0 \tilde{q} - 2C_2 \cos q_0 \frac{\tilde{q}^2}{2} + 2C_2 \sin q_0 \frac{\tilde{q}^3}{6} + 2C_2 \cos q_0 \frac{\tilde{q}^4}{24}$$

Applying the inverse Fourier transform to Eq. (A1) and taking into account that if $\phi_{\tilde{k},\tilde{q}}$ is a Fourier image of the function $\phi(z,n,t)$, then $\tilde{k}\phi_{\tilde{k},\tilde{q}}$ is the Fourier image of the quantity $-i\frac{\partial \phi}{\partial z}$, $\tilde{q}^m \phi_{\tilde{k},\tilde{q}} \leftrightarrow (-i)^m \frac{\partial^{(m)}\phi}{\partial n^{(m)}}$ $(m = 1, \ldots, 4)$, and $\omega_{\tilde{k},\tilde{q}}\phi_{\tilde{k},\tilde{q}} \leftrightarrow i\frac{\partial \phi}{\partial t}$,

respectively, it is easy to obtain Eq. (9). Note that for the slowly varying amplitudes $\phi(z,n,t)$ and $\psi(z,n,t)$ we can introduce the generalized transverse continuous coordinate x instead of discrete n. The terms with ν can be vanished by an ordinary phase transformation.

[1] T. Pertsch, T. Zentgraf, U. Peschel, A. Bräuer, and F. Lederer, Anomalous Refraction and Diffraction in Discrete Optical Systems, Phys. Rev. Lett. **88**, 093901 (2002).

[2] H. S. Eisenberg, Y. Silberberg, R. Morandotti, and J. S. Aitchison, Diffraction Management, Phys. Rev. Lett. **85**, 1863 (2000).

[3] H. Kosaka, T. Kawashima, A. Tomita, M. Notomi, T. Tamamura, T. Sato, and S. Kawakami, Self-collimating phenomena in photonic crystals, Appl. Phys. Lett. **74**, 1212 (1999).

[4] R. Morandotti, H. S. Eisenberg, Y. Silberberg, M. Sorel, and J. S. Aitchison, Self-Focusing and Defocusing in Waveguide Arrays, Phys. Rev. Lett. **86**, 3296 (2001).

[5] Yu. S. Kivshar, Self-localization in arrays of defocusing waveguides, Opt. Lett. **18**, 1147 (1993).

[6] D. N. Christodoulides and R. I. Joseph, Discrete self-focusing in nonlinear arrays of coupled waveguides, Opt. Lett. **13**, 794 (1988).

[7] R. Morandotti, D. Mandelik, Y. Silberberg, J. S. Aitchison, M. Sorel, D. N. Christodoulides, A. A. Sukhorukov, and Yu. S. Kivshar, Observation of discrete gap solitons in binary waveguide arrays, Opt. Lett. **29**, 2890 (2004).

[8] Y. Kominis, Analytical solitary wave solutions of the nonlinear Kronig-Penney model in photonic structures, Phys. Rev. E **73**, 066619 (2006).

[9] Y. Kominis and K. Hizanidis, Lattice solitons in self-defocusing optical media: Analytical solutions of the nonlinear Kronig-Penney model, Opt. Lett. **31**, 2888 (2006).

[10] Y. Kominis, A. Papadopoulos, and K. Hizanidis, Surface solitons in waveguide arrays: Analytical solutions, Opt. Express **15**, 10041 (2007).

[11] K. Hizanidis, Y. Kominis, and N. Efremidis, Interlaced linear-nonlinear optical waveguide arrays, Opt. Express **16**, 18296 (2008).

[12] B. A. Malomed, D. J. Kaup, and R. A. Van Gorder, Unstaggered-staggered solitons in two-component discrete nonlinear Schrödinger lattices, Phys. Rev. E **85**, 026604 (2012).

[13] Y. Kominis, Bright, dark, antidark, and kink solitons in media with periodically alternating sign of nonlinearity, Phys. Rev. A **87**, 063849 (2013).

[14] A. Auditore, M. Conforti, C. De Angelis, T. R. Akylas, and A. B. Aceves, Dark-antidark solitons in waveguide arrays with alternating positive-negative couplings, Opt. Commun. **297**, 125 (2013).

[15] I. V. Barashenkov, L. Baker, and N. V. Alexeeva, PT-symmetry breaking in a necklace of coupled optical waveguides, Phys. Rev. A **87**, 033819 (2013).

[16] M. Conforti, C. De Angelis, and T. R. Akylas, Energy localization and transport in binary waveguide arrays, Phys. Rev. A **83**, 043822 (2011).

[17] N. K. Efremidis and D. N. Christodoulides, Discrete solitons in nonlinear zigzag optical waveguide arrays with tailored diffraction properties, Phys. Rev. E **65**, 056607 (2002).

[18] D. R. Smith, W. J. Padilla, D. C. Vier, S. C. Nemat-Nasser, and S. Schultz, Composite Medium with Simultaneously Negative Permeability and Permittivity, Phys. Rev. Lett. **84**, 4184 (2000).

[19] R. A. Shelby, D. R. Smith, S. C. Nemat-Nasser, and S. Schultz, Microwave transmission through a two-dimensional, isotropic, left-handed metamaterial, Appl. Phys. Lett. **78**, 489 (2001).

[20] R. A. Shelby, D. R. Smith, and S. Schultz, Experimental verification of a negative index of refraction, Science **292**, 77 (2001).

[21] C. G. Parazzoli, R. B. Greegor, K. Li, B. E. C. Koltenbah, and M. Tanielian, Experimental Verification and Simulation of Negative Index of Refraction Using Snell's Law, Phys. Rev. Lett. **90**, 107401 (2003).

[22] M. Bayindir, K. Aydin, E. Ozbay, P. Markoš, and C. M. Soukoulis, Transmission properties of composite metamaterials in free space, Appl. Phys. Lett. **81**, 120 (2002).

[23] P. Markoš and C. M. Soukoulis, Transmission studies of left-handed materials, Phys. Rev. B **65**, 033401 (2001); Numerical studies of left-handed materials and arrays of split ring resonators, Phys. Rev. E **65**, 036622 (2002).

[24] Shumin Xiao, V. P. Drachev, A. V. Kildishev, X. Ni, U. K. Chettiar, H-K. Yuan, and V. M. Shalaev, Loss-free and active optical negative index metamaterials, Nature **466**, 735 (2010).

[25] A. A. Zharov, I. V. Shadrivov, and Yu. S. Kivshar, Nonlinear Properties of Left-Handed Metamaterials, Phys. Rev. Lett. **91**, 037401 (2003).

[26] C. Luo, S. G. Johnson, and J. D. Joannopoulos, All-angle negative refraction in a three-dimensionally periodic photonic crystal, Appl. Phys. Lett. **81**, 2352 (2002).

[27] C. Luo, S. G. Johnson, J. D. Joannopoulos, and J. B. Pendry, All-angle negative refraction without negative effective index, Phys. Rev B **65**, 201104(R) (2002).

[28] I. V. Shadrivov, A. A. Zharov, and Yu. S. Kivshar, Second harmonic generation in nonlinear left-handed metamaterials, J. Opt. Soc. Am. B **23**, 529 (2006).

[29] A. I. Maimistov and I. R. Gabitov, Nonlinear optical effects in artificial materials, Eur. Phys. J.: Spec. Top. **147**, 265 (2007).

[30] A. K. Popov, S. A. Myslivets, and V. M. Shalaev, Coherent nonlinear-optical energy transfer and backward-wave optical parametric generation in negative-index, Physica B **405**, 2999 (2010).

[31] I. V. Shadrivov, Nonlinear guided waves and symmetry breaking in left-handed waveguides, Photonics Nanostruct.: Fundam. Appl. **2**, 175 (2004).

[32] M. W. Feise, I. V. Shadrivov, and Yu. S. Kivshar, Tunable transmission and bistability in left-handed band-gap structures, Appl. Phys. Lett. **85**, 1451 (2004).

[33] A. A. Zharov, N. A. Zharova, I. V. Shadrivov, and Yu. S. Kivshar, Subwavelength imaging with opaque nonlinear left-handed lenses, Appl. Phys. Lett. **87**, 091104 (2005).

[34] S. O. Elyutin, A. I. Maimistov, and I. R. Gabitov, On the third harmonic generation in a medium with negative pump wave refraction, JETP **111**, 157 (2010).

[35] E. I. Ostroukhova and A. I. Maimistov, Third harmonic generation in the field of a backward pump wave, Opt. Spectrosc. **112**, 255 (2012).

[36] E. I. Ostroukhova and A. I. Maimistov, Spatial distribution of the interacting wave's amplitudes under third harmonic generation in a negative-positive refractive medium, Opt. Spectrosc. **115**, 378 (2013).

[37] I. V. Shadrivov, A. A. Sukhorukov, Yu. S. Kivshar, A. A. Zharov, A. D. Boardman, and P. Egan, Nonlinear surface waves in left-handed materials, Phys. Rev. E **69**, 016617 (2004).

[38] I. V. Shadrivov, N. A. Zharova, A. A. Zharov, and Yu. S. Kivshar, Defect modes and transmission properties of left-handed bandgap structures, Phys. Rev. E **70**, 046615 (2004).

[39] I. V. Shadrivov, R. W. Ziolkowski, A. A. Zharov, and Yu. S. Kivshar, Excitation of guided waves in layered structures with negative refraction, Opt. Express **13**, 481 (2005).

[40] N. A. Zharova, I. V. Shadrivov, A. A. Zharov, and Yu. S. Kivshar, Nonlinear transmission and spatiotemporal solitons in

[41] metamaterials with negative refraction, Opt. Express **13**, 1291 (2005).

[41] I. V. Shadrivov, A. A. Sukhorukov, and Yu. S. Kivshar, Guided modes in negative-refractive-index waveguides, Phys. Rev. E **67**, 057602 (2003).

[42] N. M. Litchinitser, I. R. Gabitov, and A. I. Maimistov, Optical Bistability in a Nonlinear Optical Coupler with a Negative Index Channel, Phys. Rev. Lett. **99**, 113902 (2007).

[43] E. V. Kazantseva, A. I. Maimistov, and S. S. Ozhenko, Solitary electromagnetic wave propagation in the asymmetric oppositely directed coupler, Phys. Rev. A **80**, 043833 (2009).

[44] Y. Xiang, S. Wen, X. Dai, and D. Fan, Modulation instability in nonlinear oppositely directed coupler with a negative-index metamaterial channel, Phys. Rev. E **82**, 056605 (2010).

[45] B. Dana, A. Bahabad, and B. A. Malomed, CP symmetry in optical systems, Phys. Rev. A **91**, 043808 (2015).

[46] D. A. Zezyulin, V. V. Konotop, and F. K. Abdullaev, Discrete solitons in arrays of positive and negative index waveguides, Opt. Lett. **37**, 3930 (2012).

[47] A. A. Dovgiy and A. I. Maimistov, Solitary waves in a binary nonlinear waveguide array, Opt. Spectrosc. **116**, 626 (2014).

[48] L. Zhang, Y. Xiang, X. Dai, and S Wen, Modulation instability in an array of positive- and negative-index waveguides, J. Opt. Soc. Am. B **31**, 3029 (2014).

[49] E. V. Kazantseva and A. I. Maimistov, Nonlinear waves in an array of zigzag waveguides with alternating positive and negative refractive indices, Quantum Electron. **43**, 807 (2013).

[50] A. A. Dovgiy, Modulation instability in a zigzag array of nonlinear waveguides with alternating positive and negative refractive indices, Quantum Electron. **44**, 1119 (2014).

[51] A. A. Sukhorukov, A. S. Solntsev, S. S. Kruk, D. N. Neshev, and Yu. S. Kivshar, Nonlinear coupled-mode theory for periodic plasmonic waveguides and metamaterials with loss and gain, Opt. Lett. **39**, 462 (2014).